Journal of Cell Science 108, 2963-2972 (1995)
Printed in Great Britain © The Company of Biologists Limited 1995
JCS3165

Mapping of nucleoporins to the center of the nuclear pore complex by post-embedding immunogold electron microscopy

Monika Grote*, Ulrich Kubitscheck, Rudolf Reichelt and Reiner Peters

Institut für Medizinische Physik und Biophysik, Westfälische Wilhelms-Universität, Robert-Koch-Strasse 31, 48149 Münster, Germany

*Author for correspondence

SUMMARY

Ultrathin sections of Lowicryl K4M embedded cultured 3T3 cells, human keratinocytes and mouse/rat liver tissue were incubated with polyspecific primary antibodies against p62 and other nucleoporins followed by 10 nm gold labeled secondary antibodies. By quantitatively evaluating both cross sections and tangential sections of the NPC, we found that irrespective of the cell type antibodies predominantly bound within a radius of 25 nm around the central axis of the nuclear pore complex (NPC). Superposition of a current structural model of the NPC with the nucleoporin distribution observed by us showed that nucleoporins mapped predominantly to the controversely discussed 'central granule'. Our experimental approach was verified by mapping gp210, another nuclear pore protein, at or very close to the NPC in the perinuclear cisterna thus establishing a distribution pattern completely different from that of the nucleoporins.

Key words: nuclear pore complex, transporter, nucleoporin, post-embedding immunogold localization, quantitative evaluation

INTRODUCTION

An intensive and well co-ordinated transport of proteins and ribonucleoprotein particles (RNP) between cell nucleus, containing the genetic material, and the cytoplasm, harboring the protein synthesizing apparatus, is vital for the cell. The nuclear envelope serves this purpose. On the one hand, it effectively separates the nuclear contents from the cytoplasm. On the other hand, it provides, by virtue of the nuclear pore complex (NPC), the basis for the controlled nucleo-cytoplasmic exchange.

The NPC is a very large and highly complex macromolecular assembly. It has an overall cylindrical shape with a radius of approximately 60 nm and a height of 70 nm (Unwin and Milligan, 1982; Hinshaw et al., 1992; Akey and Radermacher, 1993). The wall of this cylinder, referred to as the basic framework by Hinshaw et al. (1992), is approximately 35 nm thick and thus creates a central channel of about 25 nm radius. Filaments radiate from both faces of the NPC into the cytoplasm and nuclear volume, respectively. The cytoplasmic filaments are shorter and not connected to each other while the nuclear filaments are longer and form a basket or 'fishtrap' (Jarnik and Aebi, 1991; Ris, 1991; Ris and Malecki, 1993).

Whereas there is general agreement about the basic structural components of the NPC and their masses (Reichelt et al., 1990), details concerning the composition and arrangement of individual elements remain controversial. Thus, according to Akey and Radermacher (1993) the central channel is occupied by the 'transporter', a double-barrel-shaped structure previously referred to as the central granule (cf. Scheer et al., 1988). Intriguingly, in specimens prepared for electron microscopy only a fraction of NPCs contains a central granule. The fraction of central granule-containing NPCs is very variable between different preparations of the same cell type and between different cell types (for review of early studies, see Maul, 1977). Most recently, Panté and Aebi (1994a) reported that in nuclear envelopes isolated manually from *Xenopus laevis* oocytes the frequency of NPC attached central granules is increased by prior treatment with Cu^{2+}-orthophenantroline but decreased in the presence of ATP. For these and other reasons it has been speculated (cf. Maul, 1977) that the central granule may not be a genuine permanent component of the NPC but rather a RNP in transit. This hypothesis was supported recently by suggesting that the central granule is built up from a special RNP species referred to as the 'vault' (Kedersha et al., 1991). Alternatively, Panté and Aebi (1994a) have suggested that the central granule may be generated from collapsed filaments, especially the terminal ring of the nuclear basket. Yet the rather trivial possibility remains that the removal of the central granule is simply a preparation artifact.

The identity and nature of the central granule has profound implications for the mechanism(s) of nucleo-cytoplasmic transport. If the central granule is a genuine permanent component of the NPC it presumably constitutes the actual transport site. Specifically, Akey (1990) has suggested that the central granule has the function of a 'molecular lock' with a channel of adjustable width and gates on both the cytoplasmic and the nuclear face. Others (Berrios et al., 1991) have suggested that nucleo-cytoplasmic transport occurs on filaments traversing the NPC. Alternatively, Kedersha et al. (1991) have

proposed that 'vaults' mentioned above function as a type of container transporting a macromolecular cargo through the NPC. Recently, the central granule has been envisioned as a 'plug', being 'pulled' to permit transit of macromolecules through the central channel of the NPC (Panté and Aebi, 1993).

Nucleoporins are a class of proteins occurring specifically in the NPC (for a review of NPC proteins and definition of nomenclature see Panté and Aebi, 1994b). A typical nucleoporin such as p62 (Starr et al., 1990; Carmo-Fonseca et al., 1991; Cordes et al., 1991) has a domain structure with an N terminus containing multiple copies of the pentapeptide motif XFXFG and a C terminus rich in heptad repeats characteristic for coiled-coil conformation. In addition, p62 is modified (Davis and Blobel, 1987) at up to 20 sites with O-linked *N*-acetylglucosamine (GlcNac). Immunoferritin and immunogold electron microscopy has been frequently employed to map nucleoporins of the NPC. However, all of these studies - with only a single exception (Aris and Blobel, 1989) - employed the pre-embedding approach, i.e. a procedure in which suitably permeabilized cells or thick cryosections are labeled with the primary and secondary antibodies prior to embedding and ultrathin sectioning. Thus, using the monoclonal antibody MAb 414 which recognizes p62 as well as a number of other nucleoporins, Davis and Blobel (1986) mapped nucleoporins to the outer face of the NPC in permeabilized rat liver nuclei. Akey and Goldfarb (1989) reported that nucleoporin epitopes of the *Xenopus* oocyte NPC were strongly concentrated over the central granule on the cytoplasmic face. Using a polyclonal anti-nucleoporin antibody generated in guinea pig, Cordes et al. (1991) mapped nucleoporins to both the nucleo- and cytoplasmic face of the mouse liver NPC. In *Xenopus* ovary, however, only the nucleoplasmic face of the NPC was decorated, suggesting a species-specific distribution of nucleoporins. Applying the antibody generated by Cordes et al. (1991), Panté and Aebi (1993) localized nucleoporin-immunoreactivity to the terminal ring of the nuclear basket.

In the present study we have employed post-embedding immunogold electron microscopy, a well-known method in which cells or tissue are first fixed, embedded and ultrathin sectioned and subsequently labeled with antibodies. Thus, in contrast to the pre-embedding approach, internal epitopes which are masked in native or freeze-dried specimen become accessible. Using both a monoclonal (MAb 414) and a polyclonal (kindly donated by G. Krohne, Würzburg) anti-nucleoporin antibody we mapped antigenic sites of the NPC in tangential and cross sections of the nuclear envelopes in 3T3 cells, keratinocytes and mouse/rat liver tissue. We found in all of these cases that nucleoporins were predominantly localized in the central region of the NPC. From a comparison of our data with a structural model of the NPC (Hinshaw et al., 1992) it became obvious that nucleoporins mapped predominantly to the central granule. This finding suggests that the central granule is a genuine component of the NPC and thus supports the view (e.g. Akey, 1990) that the central granule is the actual site of macromolecular transport across the NPC.

MATERIALS AND METHODS

Antibodies

The monoclonal antibody MAb 414 which is specific for p62 and a number of other nucleoporins was obtained from BAbCO (Berkeley Antibody Company, Richmond, CA, USA; Cat. No. MMS - 120P, Lot No. 717 11 002). A polyclonal antibody raised against rat p62 in guinea pig (cf. Cordes et al., 1991) was kindly donated by Dr Georg Krohne (Würzburg, Germany). This antibody is specific for p62 and other nucleoporins, similar to MAb 414. RL20 monoclonal antibody was a gift from Dr Larry Gerace (La Jolla, California, USA). It is directed against the nuclear pore membrane protein gp210 (cf. Greber et al., 1990) and was used in a methodical control experiment. In immunological control experiments either a monoclonal antibody of irrelevant specificity, namely for timothy grass pollen allergen *Phl p* V (gift of Dr Valenta, Vienna, Austria), or a normal guinea pig serum (Dakopatts, Hamburg, Germany) was employed. Goat anti-mouse IgG coupled to 10 nm colloidal gold particles (GAM IgG 10), goat anti-guinea pig IgG coupled to 10 nm colloidal gold particles (GAG 10) or Protein A/G coupled to 10 nm colloidal gold particles (PAG 10) were used as secondary antibodies (British BioCell, distributed by Plano, Marburg, Germany).

Cells and tissue

3T3 cells were cultured in DMEM complete medium (Boehringer, Mannheim, Germany) at 37°C at 5% CO_2 and passaged every three days. Human keratinocytes (A 431 ATCC) were cultivated in RPMI 1640 culture medium (Gibco, Uxbridge, UK) with the addition of 5% fetal calf serum at 5% CO_2 according to standard procedures. Mouse liver tissue was obtained from a six-week-old female Balb/c mouse. Rat liver tissue was taken from a two-month-old male Wistar rat.

Fixation, embedding and sectioning

For post-embedding labeling, cultured cells, detached from the culture vessels by trypsinisation, and mouse/rat liver tissue (cubes of approx. 1 mm^3) were fixed in freshly prepared 4% *p*-formaldehyde + 0.5% glutaraldehyde in 0.1 M sodium cacodylate buffer at pH 7.3 for 1 hour at room temperature. Dehydration and embedding of the samples into Lowicryl K4M resin were performed according to Carlemalm et al. (1982) with modifications: After washing in the fixation buffer, the cells were dehydrated through a graded series of ethanols. The dehydrated samples were infiltrated with three mixtures of ethanol:Lowicryl K4M resin (2:1, 1:1, 1:2) staying 4 hours at each stage. Afterwards, they were transferred into the pure Lowicryl K4M resin for 36 hours with one exchange of the medium after 18 hours (all these steps at room temperature). The samples were then placed into fresh embedding medium and cooled down to –35°C within a time period of 4 hours. Polymerisation was achieved by irradiation with ultraviolet light for 24 hours and continued for another day at room temperature. Ultrathin sections (silver color) were cut and placed on Pioloform-coated nickel grids.

For pre-embedding labeling, cells were permeabilized and incubated with antibodies (see below). The cells were then fixed in 2.5% glutaraldehyde in 0.1 M Sörensen phosphate buffer, pH 7.3, overnight at 4°C and detached from the culture vessel by gently shaking. Cells in suspension were postfixed in 1% OsO_4 in 0.1 M Sörensen phosphate buffer, pH 7.3, for 1.5 hours at room temperature, dehydrated in ethanol and embedded in Spurr's resin according to standard procedures.

Immunolabeling

In the case of the post-embedding procedure ultrathin sections were placed on nickel grids and incubated face down on drops of the following solutions in a moist chamber at room temperature (buffers: PBS, pH 7.4; Tris-BSA, pH 8.2): (i) 5% BSA in PBS, 15 minutes. (ii) MAb 414, diluted 1:500 in PBS, or the polyclonal anti-p62 antibody, diluted 1:5 in PBS, 2 hours. (iii) PBS (twice), Tris-BSA (once). (iv) GAM IgG 10, diluted 1:10 in Tris-BSA (in the case of specimens labeled with MAb 414) or GAG 10, diluted 1:40 in Tris-BSA (in the case of specimens labeled with the polyclonal anti-p62 antibody), 1 hour. In some experiments, specimens labeled with either MAb 414 or

the polyclonal anti-p62 antibody were incubated with PAG 10, diluted 1:20 in Tris-BSA, 1 hour. (v) Tris-BSA (once), distilled water (twice).

In the case of the pre-embedding procedure 3T3 cells were permeabilized with digitonin according to the method of Adam et al. (1990), incubated with MAb 414, diluted 1:3,000 in PBS buffer, pH 7.4, for 30 minutes, washed in PBS, incubated with GAM IgG 10, diluted 1:10 in PBS for 30 minutes and washed again in PBS (all labeling steps were performed at 4°C). Fixation and embedding in Spurr's resin was as described above.

RL20 monoclonal antibody was supplied at an original concentration of 7.5 mg/ml. It was used for labeling experiments at a dilution of 1:500 in PBS buffer, pH 7.4. The labeling protocol was similar to that of MAb 414.

In control experiments MAb 414 and RL20 monoclonal antibody were replaced by the monoclonal anti-*Phl p* V antibody described above and the polyclonal anti-p62 antibody was replaced by normal guinea pig serum. In addition, experiments were carried out in which the specific primary antibody was omitted and sections were only incubated with the gold-conjugated secondary antibody.

Staining, electron microscopy and documentation

After post-embedding labeling, sections were stained with uranyl acetate for 3 minutes and lead citrate for 2 seconds. After pre-embedding labeling, sections were stained with uranyl acetate for 30 minutes and lead citrate for 8 minutes. Stained sections were examined in a Hitachi H500 transmission electron microscope operated at 75 kV. The magnification of the microscope was calibrated using latex spheres of different sizes. Photographs were taken on Agfa Gevaert 23D56 films.

Mapping of gold particles

For quantitatively mapping immunogold particles to the NPC only such NPCs were considered which had been cut either perpendicularly with respect to the nuclear surface or in-plane with the nuclear envelope. Examples of such NPCs are given in Figs 1-3.

For measurements micrographs were taken at a primary magnification of ×56,000 and further enlarged by a factor of two. The enlarged micrographs were used to measure the positions of gold particles with regard to the *r*,*z*-coordinate system shown in Fig. 7a and defined in the following manner: in cross sections of the nuclear envelope the inner nuclear membranes on both sites of the NPC were connected by a straight line. This constituted the *r*-axis while an axis traversing the center of the NPC perpendicular to the nuclear envelope was chosen as *z*-axis. The number of NPCs and gold particles in each type of measurement is given in the legends to Figs 4,5 and 6.

In cross sections, a pair of co-ordinates (*ri*,*zi*) was assigned to each gold particle *i*. Co-ordinate values were determined in steps of 0.5 mm which corresponded to 4.45 nm. The error in these determinations was estimated to be approximately ±2.2 nm.

Then, the frequency of gold particles was determined by counting particles within areas of 10 nm × 10 nm, i.e. counting gold particles displaying co-ordinate values (*ri*,*zi*) with $n*10 \text{ nm} \leq ri < (n+1)*10$ nm, and $m*10 \text{ nm} \leq zi < (m+1)*10$ nm (n, m = 0, 1, 2, 3...). The resulting frequency distribution was encoded by defined grey values as shown in Fig. 4 where increasing darkness corresponds to larger numbers of colloids found in the respective image areas.

In addition, the size of each nuclear pore was characterized by measuring (i) the height *h* between the inner and outer nuclear membrane parallel to the *z*-axis in the immediate neighborhood of the NPC, and (ii) the radius *r* of the hole in the nuclear envelope occupied by the NPC. Mean values were found to be $h \approx 37$ nm and $r \approx 45$ nm, irrespective of cell type and tissue. These data agree well with the values of *h*=40 nm and *r*=42-47 nm reported for the NPC of *Xenopus* oocytes (Unwin and Milligan, 1982; Reichelt et al., 1990; Hinshaw et al., 1992; Hinshaw, 1994; Akey and Radermacher, 1993). In Fig. 4 the *r*-axis coincides with the inner nuclear membrane. The position of the outer nuclear membrane and the part of the nuclear membrane joining the outer with inner nuclear membrane were indicated by a broken line.

In tangentional sections, the distance (*r*-coordinate) of each gold particle from the central axis (*z*-axis) was measured. Then, the frequency of the gold particles was determined by counting particles within rings of 10 nm around the *z*-axis (Fig. 5).

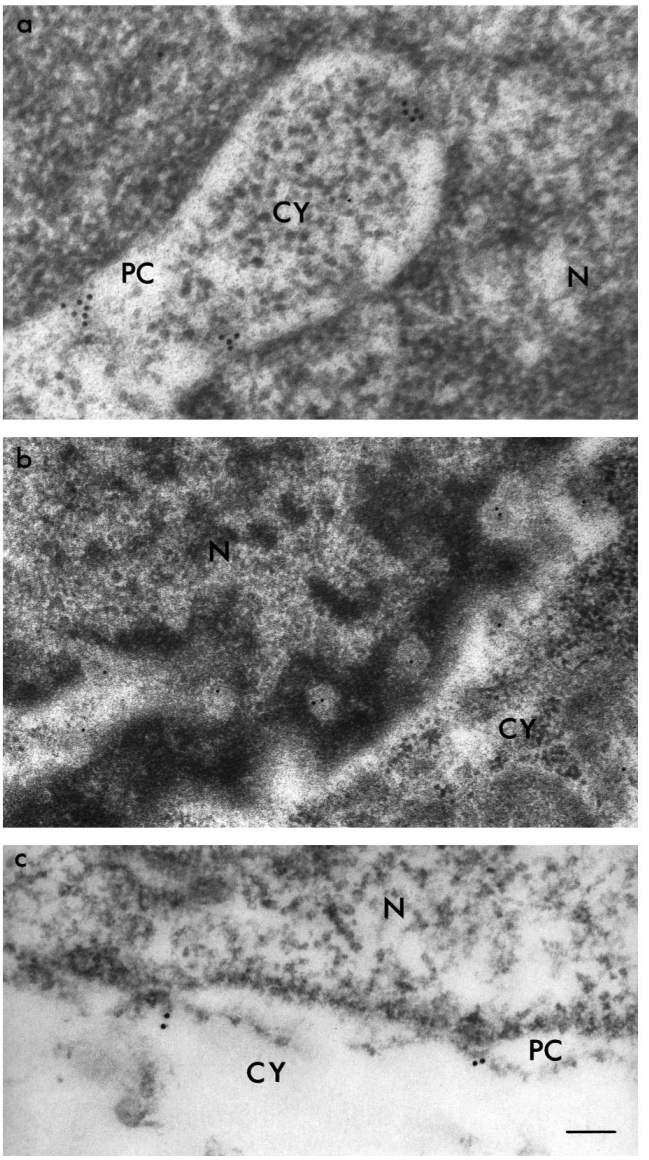

Fig. 1. Comparison of nucleoporin localization by post- and pre-embedding immune electron microscopy. (a) Ultrathin section of a human keratinocyte after post-embedding labeling with the monoclonal anti-nucleoporin antibody MAb 414 and and the gold-labeled secondary antibody GAM IgG 10, showing a cross section of nuclear envelope. Gold particles are seen to be localized in the interior of the nuclear pore complexes. (b) Ultrathin section of a 3T3 cell after post-embedding labeling with MAb 414 and GAM IgG 10, showing a tangential section of the nuclear envelope. Gold particles are localized in the center of the nuclear pore complexes. (c) Ultrathin section of 3T3 cell after permeabilization and pre-embedding labeling with MAb 414 and GAM IgG 10, showing a cross section of nuclear envelope. In this case, gold particles are found exclusively at the cytoplasmic face of the nuclear pore complexes. Bar: a,c, 90 nm; b, 150 nm; CY, cytoplasm; N, nucleus; PC, perinuclear cisterna.

RESULTS

Post-embedding immune electron microscopy mapped nucleoporins predominantly to internal regions of the NPC, in contrast to pre-embedding labeling

Fig. 1a and b give representative examples of ultrathin sections of cultured cells after post-embedding immunogold labeling and show details of the nucleus-cytoplasm area. Due to the type of fixation used, membranes including those surrounding the nucleus are not very prominent. The perinuclear cisterna, however, is clearly distinguishable.

In cross sections of the nuclear envelope (Fig. 1a), the nuclear pores appear as electron-dense bodies traversing the perinuclear space. On its nucleoplasmic face, each NPC widens into a bulbous space which is less electron-dense than the surrounding chromatin material. The cytoplasmic structures of each NPC merge into the fibrillar-granular material of the adjacent cytoplasm. Details of nuclear pore complex substructures such as nucleoplasmic and cytoplasmic fibres as determined by other electron microscopic investigation techniques are not discernible.

In tangential sections of the nuclear envelope (Fig. 1b), NPCs show more or less circular circumferences depending on the direction of cutting. Often the NPCs are surrounded by more electron-dense chromatin. Again, details of substructure can hardly be deduced from these micrographs.

In both types of section gold particles indicating the presence of nucleoporins are almost exclusively confined to the NPCs (Fig. 1a and b). If, instead of gold-labeled secondary antibodies, gold-coupled protein A/G was used for reacting with the primary antibodies, the results were principally the same but labeling sensitivity seemed somewhat reduced. So, in spite of a certain loss of immunocytochemical resolution, for qualitative illustration and quantitative evaluation only experiments using the secondary antibody method were considered. Control experiments (not shown) employing antibodies of irrelevant specificity or being performed in the absence of a primary antibody (see Materials and Methods) confirmed that non-specific labeling was negligible.

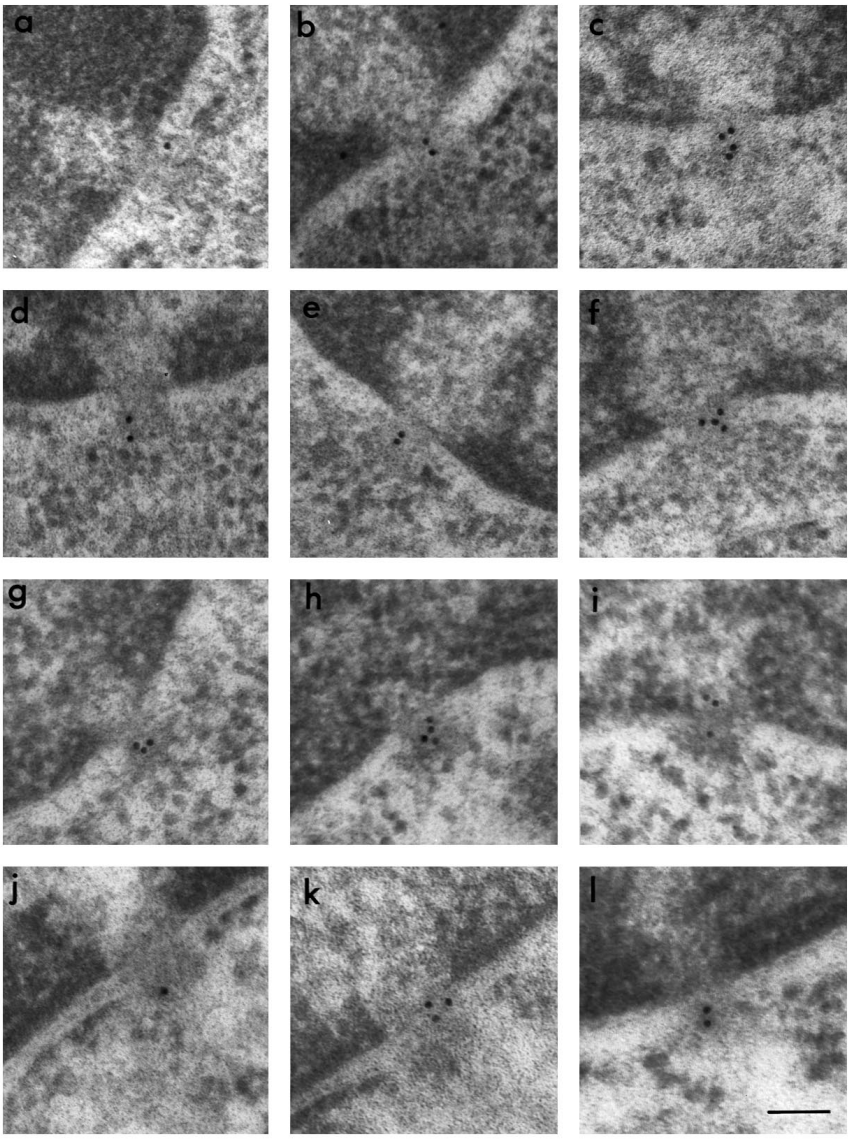

Fig. 2. Representative examples of nuclear envelope cross sections after post-embedding immunoelectron microscopy, and used to derive the distribution shown in Fig. 4. Cells and antibodies were as follows: (a-c) 3T3 cells labeled with the polyclonal anti-p62 antibody, followed by GAG 10. (d-f) 3T3 cells labeled with MAb 414, followed by GAM 10. (g-i) keratinocytes, labeled with MAb 414, followed by GAM 10. (j-l) mouse liver tissue labeled with the polyclonal anti-p62 antibody, followed by GAG 10. All micrographs show the same magnification. Bar, 90 nm.

From the cross-sections and tangential sections of the NPCs in Fig. 1a and b it was suggested that post-embedding immunogold electron microscopy mapped nucleoporins predominantly to internal regions of the NPC. Results obtained previously by pre-embedding labeling (Davis and Blobel, 1986; Akey and Goldfarb, 1989; Cordes et al., 1991; Panté and Aebi, 1993) localized nucleoporins such as p62 to external regions of the NPC. We confirmed their results by also performing a pre-embedding experiment: 3T3 cells were permeabilized and incubated with MAb 414 and gold-conjugated secondary antibody, prior to embedding and ultrathin sectioning. As shown on the cross-sections in Fig. 1c, gold particles were observed on the cytoplasmic face of the NPC. In virtually no case were gold particles observed labeling the center of the nuclear pore or its nucleoplasmic face.

Fig. 2 shows a gallery of individual cross-sectioned gold-decorated NPCs being representative for the different types of experiments, i.e. for 3T3 cells labeled with the polyclonal anti-p62 antibody (a-c), for 3T3 cells labeled with the monoclonal antibody MAb 414 (d-f), for keratinocytes labeled with MAb 414 (g-i), and for mouse liver tissue labeled with the polyclonal antibody (j-l). Examples of tangentially cut NPC are collected in Fig. 3 (a-c: 3T3 cells labeled with MAb 141; d-f: 3T3 cells labeled with the polyclonal antibody; g-i: mouse liver tissue labeled with the polyclonal antibody; j-l: mouse liver tissue labeled with MAb 414).

Quantification of post-embedding labeling revealed that nucleoporins are predominantly localized in the center of the NPC

The distribution of gold particles in NPC cross-sections is shown in Fig. 4a-e. In these graphs the *r*-axis coincides with the inner nuclear membrane while the *z*-axis is identical with an axis being perpendicular to the nuclear envelope and traversing the center of the NPC. The approximate positions of the cytoplasmic and nuclear surfaces of the NPC are indicated by dotted lines. The position of the nuclear membrane is outlined by broken lines. The frequency of gold particles (particles per area of 10 nm × 10 nm) was encoded by grey levels as indicated in Fig. 4a.

Fig. 4a,b is based on labeling 3T3 or human keratinocytes,

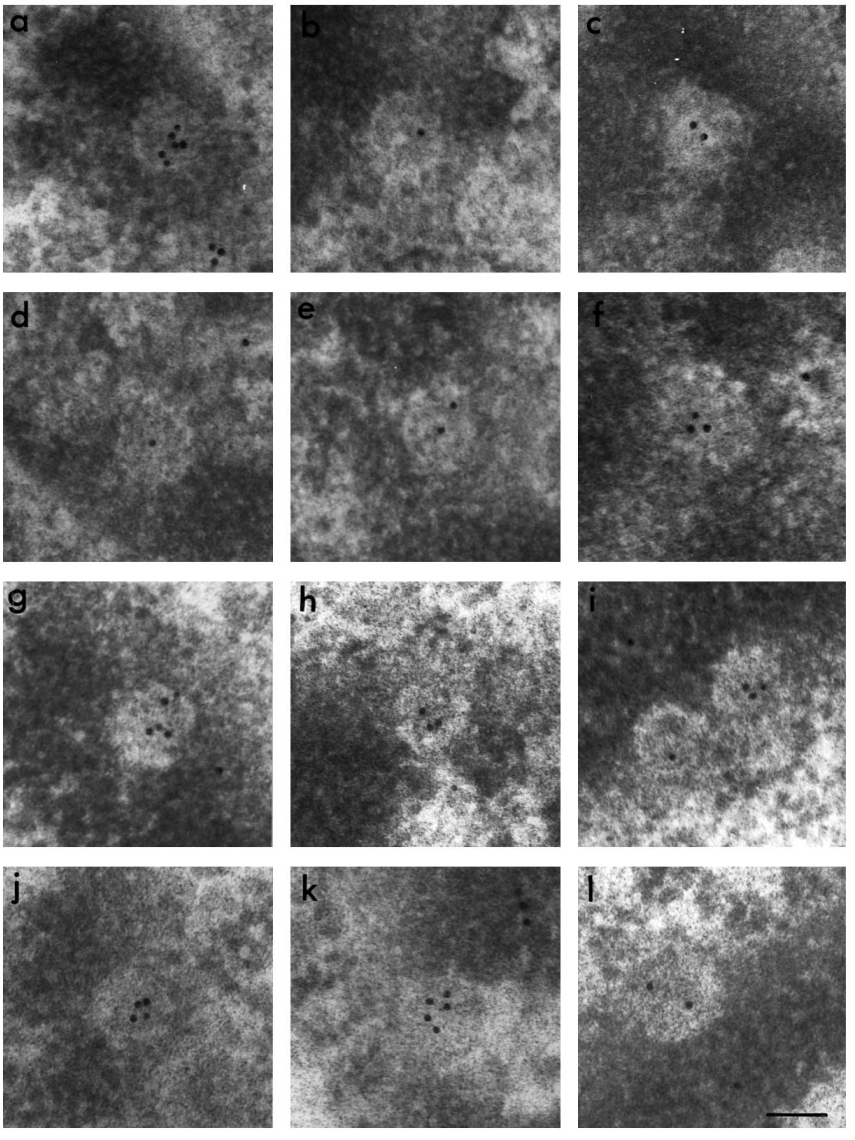

Fig. 3. Representative examples of tangential sections of the nuclear envelope after post-embedding immune electron microscopy, and used to derive the distribution shown in Fig. 5. (a-c) 3T3 cells labeled with MAb 414, followed by GAM 10. (d-f) 3T3 cells labeled with the polyclonal anti-p62 antibody, followed by GAG 10. (g-i) mouse liver tissue labeled with the polyclonal anti-p62 antibody, followed by GAG 10. (j-l) mouse liver tissue labeled with MAb 414, followed by GAM 10. All micrographs show the same magnification. Bar, 90 nm.

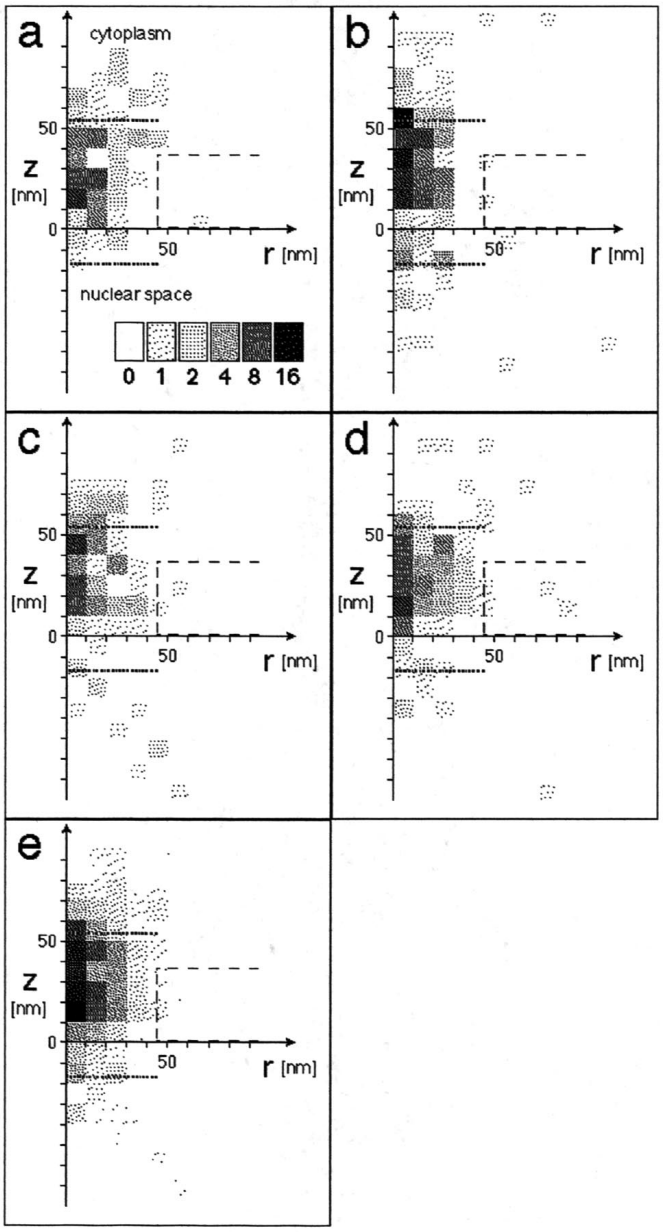

Fig. 4. Distribution of gold particles in cross-sectioned nuclear pore complexes, derived by quantification of electron micrographs as shown in Fig. 2. The *r*-axis coincides with the inner nuclear membrane, the *z*-axis is identical with the central symmetry axis of the NPC. The cytoplasmic and nuclear surface of the nuclear pore complex are indicated by dots, the nuclear membrane by broken lines. The frequency of gold particles (number per area of 10 nm × 10 nm) is encoded by the grey value scale in (a). Cells and antibodies were as follows: (a) 3T3 cells, MAb 414, GAM 10. (b) keratinocytes, MAb 414, GAM 10. (c) mouse liver tissue, polyclonal anti-p62 antibody, GAG 10. (d) 3T3 cells, polyclonal anti-p62 antibody, GAG 10. The average of (a-d) is given in (e). Total numbers of evaluated nuclear pore complexes and gold particles, respectively, were: (a) 39 and 100, (b) 44 and 162, (c) 45 and 105, (d) 52 and 115.

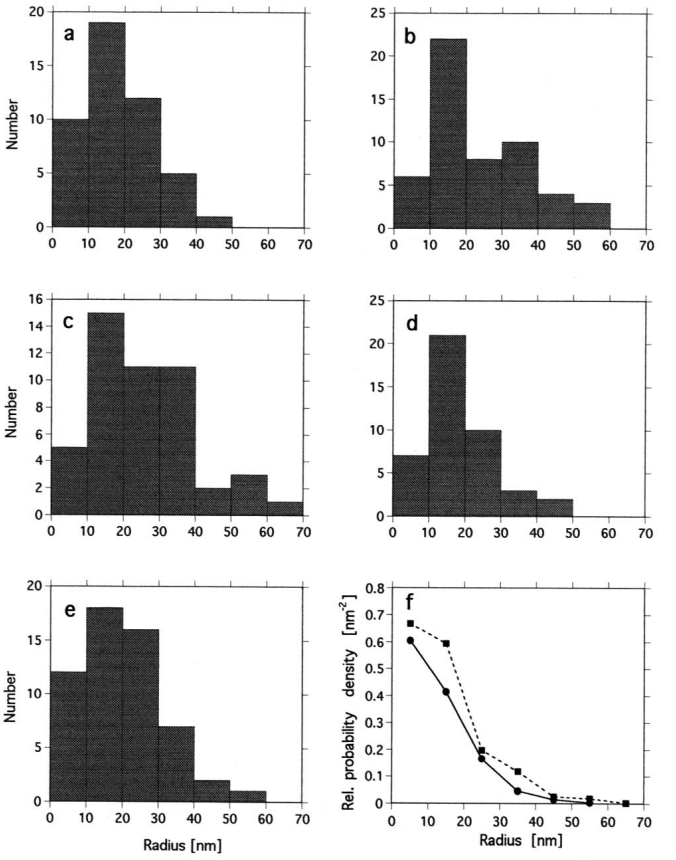

Fig. 5. Distribution of gold particles in tangential sections of the nuclear pore complex, derived by quantification of electron micrographs as shown in Fig. 3. The histograms show the radial frequency of gold particles, i.e. the number of particles counted in 10 nm thick rings around the central axis of the NPC. Cells and antibodies were as follows: (a) 3T3 cells, MAb 414, GAM 10. (b) keratinocytes, MAb 414, GAM 10. (c) mouse liver, MAb 414, GAM 10. (d) 3T3 cells, polyclonal anti-p62, GAG 10. (e) mouse liver, polyclonal anti-p62, GAG 10. In (f) the particle density, i.e. the radial frequency divided by the appropriate radius, is plotted. The broken line refers to the averaged data based on labeling with the monoclonal antibody (a-c), while the full line pertains to data based on labeling with the polyclonal antibody (d,e). Total numbers of evaluated nuclear pore complexes and gold particles, respectively, were: (a) 18 and 46, (b) 24 and 53, (c) 18 and 48, (d) 19 and 43, (e) 22 and 56.

respectively, with MAb 414 while Fig. 4c,d gives the results for experiments employing the polyclonal anti-p62 antibody to mouse liver or 3T3 cells, respectively. Fig. 4e represents an average of Fig. 4a-d showing the averaged density of the gold particle distribution.

The data for the different kinds of cells and antibodies (Fig. 4a-d) and, even more clearly, the averaged data (Fig. 4e) showed that nucleoporins were strongly concentrated in the center of the NPC. Most gold particles were found within a radius of 10 nm and very few outside a radius of 30 nm around the central axis. A few particles were also found outside the NPC, on its cytoplasmic and nuclear faces.

Results for the distribution of gold particles in tangential sections are given in Fig. 5a-f. In these histograms the frequency of gold particles occurring within a given radius around the central axis is plotted. Fig. 5a-c pertains to experiments in which 3T3 cells, human keratinocytes, or mouse liver, respectively, were labeled with MAb 414. Fig. 5d,e gives the

results of experiments employing the polyclonal anti-p62 antibody to 3T3 cells and mouse liver, respectively. In Fig. 5f the data of Fig. 5a-e were averaged and converted into density by dividing the frequency by the appropriate radius.

Similar to the results for cross-sections the distribution of gold particles in tangential sections shows that nucleoporins are concentrated around the central axis of the NPC. The relative density (Fig. 5f) was highest in the center of the NPC decreasing steeply with increasing radius and falling below 0.15 at a radius of ≥30 nm.

Quantification of post-embedding labeling of gp210, another nuclear pore protein, gave a distribution pattern different from that of the nucleoporins

In Fig. 6, qualitative and quantitative results of post-embedding labeling rat liver tissue with the RL20 anti-gp210 antibody are summarized. For the matter of direct comparison, MAb 414 was also applied to rat liver sections.

As the gallery of cross sections (Fig. 6a-c) shows, typical binding sites of the RL20 antibody occur at or very near nuclear pore complexes. After labeling rat liver sections with

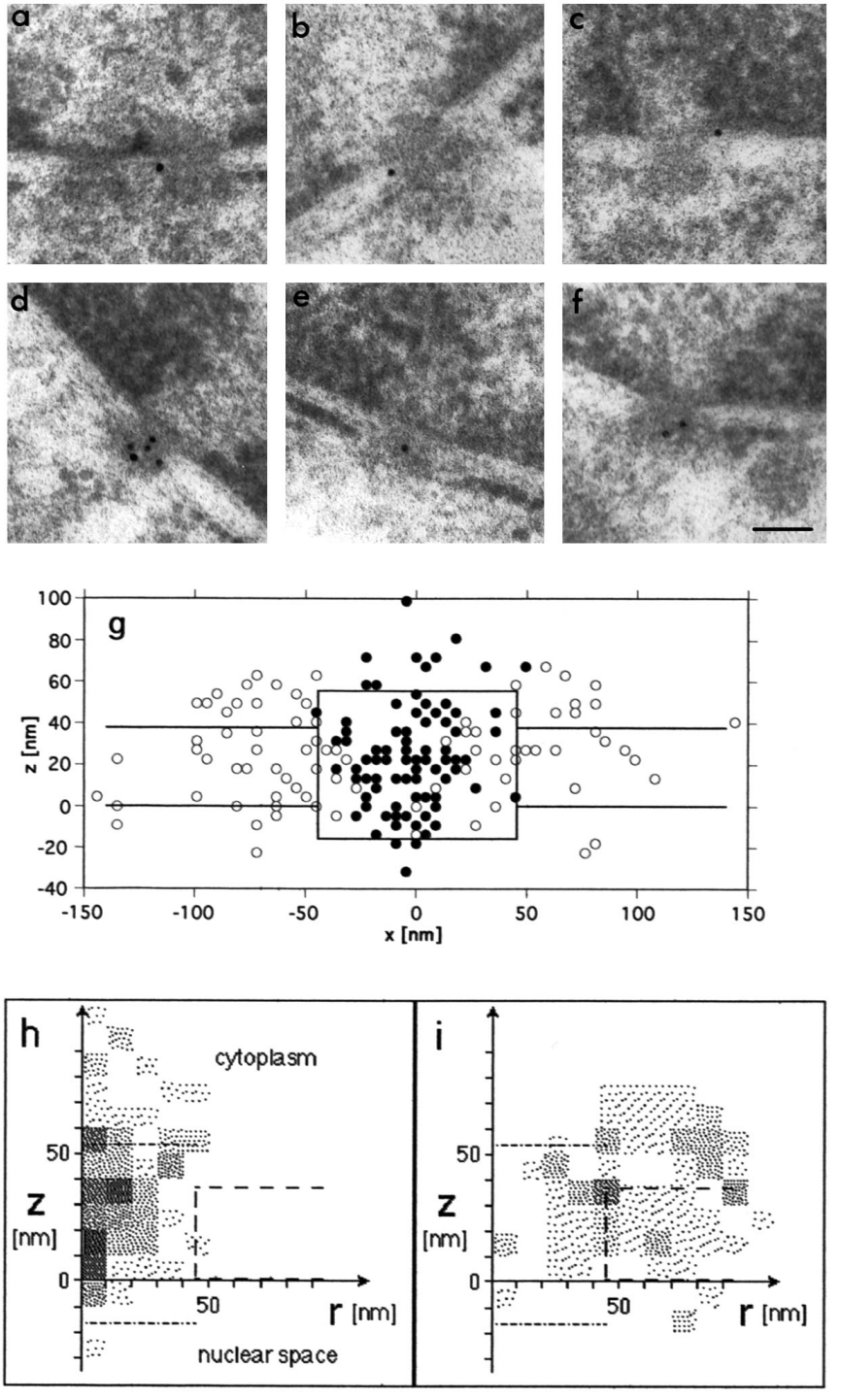

Fig. 6. Localization of gold particles in ultrathin sections of rat liver tissue after incubation with antibody RL20 and MAb 414, respectively. (a-c) Gallery of representative cross-sectioned NPCs after labeling with anti-gp210 antibody RL20, followed by GAM 10. (d-f) Gallery of representative cross-sectioned NPCs after labeling with MAb 414, followed by GAM 10. All micrographs show the same magnification with the bar corresponding to 90 nm. (g) Diagram showing simultaneously the distribution of MAb 414 binding sites (filled circles) and RL20 antibody binding sites (open circles) within the NPC and the perinuclear space (rectangle = NPC, inner nuclear membrane: z=0, outer nuclear membrane: z=37). (h) Quantitative evaluation of the distribution of gold particles in the experiments shown in d-f (MAb 414). (i) Quantitative evaluation of the distribution of gold particles in the experiments shown in a-c (RL20 antibody). Preparation and designation of diagrams in h and i was as outlined for Fig. 4. Total number of evaluated nuclear pore complexes and gold particles, respectively, were: (g) 75 and 86, (h) 44 and 103.

MAb 414 antibody (Fig. 6d-f), cross sections of nuclear pores are gold-decorated preferentially along their cylindrical axis.

A diagram showing simultaneously the binding sites of both antibodies, RL20 and 414, is presented in Fig. 6g. Antibodies binding to nucleoporins accumulate in the center of the NPC (filled circles), while gp210 concentrates at the periphery and outside the NPC in the perinuclear cisterna (open circles) (rectangle = NPC, inner nuclear membrane: z=0, outer nuclear membrane: z=37). Fig. 6h and i show the quantitative evaluation of both experiments which were performed according to Fig. 4. Again, the nucleoporins (Fig. 6h) concentrate in the central part of the NPC (within a radius of 30 nm around the central axis of the pore), while gold particles indicating the presence of gp210 (Fig. 6i) are localized in an area extending from 40 to 100 nm away from the center of the pore. Some gp210 immunoreactivity is found outside the nuclear membranes at the cytoplasmic face of the NPC.

DISCUSSION

In the present study the ultrastructural localization of nucleoporins, a class of proteins occurring only in the NPC, was investigated by post-embedding immunogold electron microscopy. In this method cells or tissues are first chemically fixed and resin embedded, then sectioned, and finally incubated with antibodies. Although this is a well-established, thoroughly characterized and frequently used method (Robards and Wilson, 1993) it has been rarely applied in recent times to study the NPC. In contrast, the NPC has been frequently investigated by pre-embedding immunoelectron microscopy in which isolated nuclear envelopes, permeabilized cells or thick cryosections are labeled with antibodies prior to embedding and ultrathin sectioning. However, the post-embedding approach can be advantageous in some instances. Obviously, by the post-embedding method, internal epitopes not accessible to antibodies in the native or freeze-dried specimen are exposed and thus become recognizable by the labeling probe. In the present case this has yielded new information on the distribution of nucleoporins within the NPC supplementing previous results obtained by pre-embedding electron microscopy and other methods.

Kellenberger and Hayat (1991) determined that in indirect immunogold cytochemistry using the secondary antibody method the distance between the labeled epitope and the gold label itself may amount to ≤25 nm. This is, of course, only a moderate precision of co-ordination. Nevertheless, it was sufficient, as our results show, to derive new information about the distribution of nucleoporins in the NPC. Future labeling studies, however, will be performed using considerably shorter immunocytochemical probes.

To preserve antigenicity, often relatively 'poor' fixation conditions have to be used. In many cases, fixation in *p*-formaldehyde supplemented with a low amount of glutaraldehyde - as in the present study - is considered to be a good compromise. However, it cannot be completely excluded that rearrangement of molecular components of the NPC occurred under these conditions. In any case, fixation conditions were identical for all the different cell types and antibodies used thus in all experiments keeping equal the error potentially arising from poor structural preservation.

The NPC has an overall cylindrical shape with a radius of approximately 60 nm and a height of 70 nm. The wall of this cylinder, the 'basic framework' (Hinshaw et al., 1992; Hinshaw, 1994) is approximately 35 nm thick leaving a central channel of about 25 nm radius. We found in cross sections (Figs 2,4) that the large majority of nucleoporin epitopes was localized within a central region of the NPC measuring about 20-30 nm × 50 nm (radius × height). Similarly, in tangential sections (Figs 3,5) we observed that nucleoporin epitopes were concentrated in the center of the NPC while the density of labeled sites steeply decreased between a radius of 20-30 nm. The averaged distributions (Figs 4e or 5f, respectively) are superimposed in Fig. 7 onto the three-dimensional model of the *Xenopus* oocyte NPC derived by Hinshaw et al. (1992). This reveals that nucleoporins occur predominantly in the

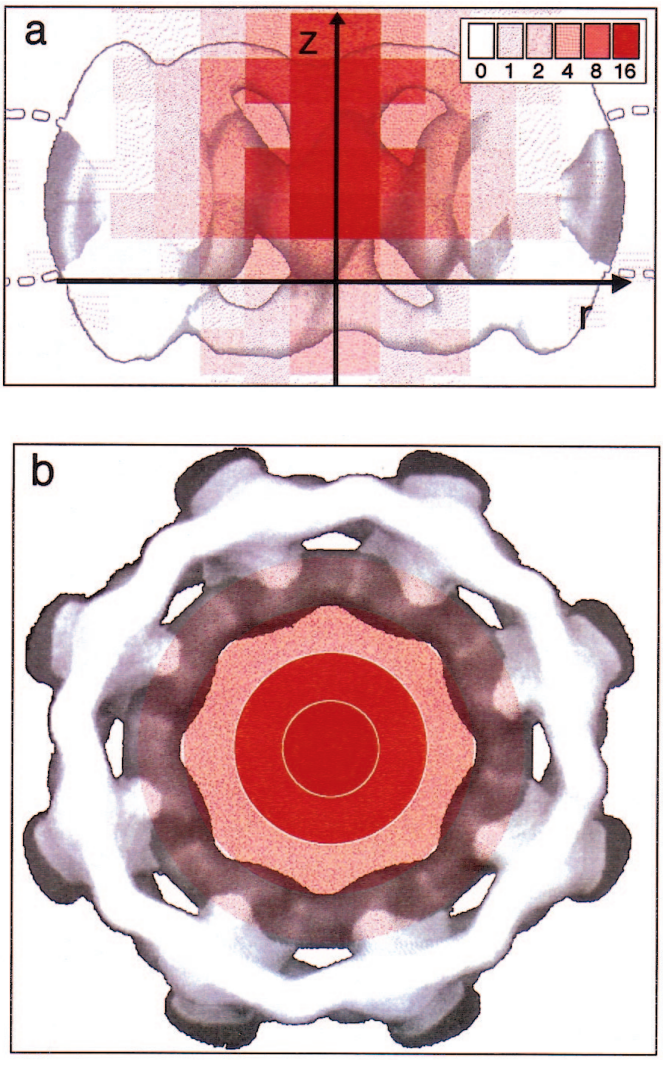

Fig. 7. Distribution of antigenic nucleoporin sites with regard to the three-dimensional model of the *Xenopus* oocyte nuclear pore complex suggested by Hinshaw and colleagues. (a) Combination of the averaged cross-sectional density distribution (Fig. 4e) and the cut away side view of the NPC (Hinshaw, 1994; Fig. 2).
(b) Combination of the averaged radial density distribution (Fig. 5f) and the top view of the NPC (Hinshaw, 1994; Fig. 2). Increasing intensity in red indicates an increasing density of gold particles in the respective compartment of the NPC.

region of the central channel, a conclusion assuming that there are no gross structural differences between the *Xenopus* oocyte NPC and the one of 3T3 cells, keratinocytes and rat/mouse liver cells, which, however, seems to be justified (e.g. Maul, 1977).

Labeling experiments using an antibody directed against another nuclear pore protein, gp210, provided a kind of internal standard or methodical control in our experiments. The epitope recognized by the RL20 antibody was shown to be located close to the nuclear pore in the perinuclear cisterna (Greber et al., 1990). In detail, Greber et al. (1990) report that after use of RL20 antibody in rat liver envelopes gold labeling occurred inside the lumen of the nuclear membranes approximately 120-80 nm away from the center of the nuclear pores. Thus our post-embedding labeling approach should have revealed a distribution pattern of gp210 labels significantly different from that obtained for the nucleoporin labels. Indeed, our quantitative evaluation of a large number of nuclear pores after post-embedding RL20 immunogold labeling revealed an accumulation of gold particles at a distance of 40-100 nm from the center of the pores (Fig. 6a-c, g and i). Furthermore, we found some gold particles outside the perinuclear cisterna possibly indicating some immunoreactivity of cytoplasmic parts of the NPC which might not be obtainable when labeling isolated nuclear envelopes. In any case, there is a distinct difference between the maximum accumulation of gold particles when comparing the results obtained for the peripheral membrane protein gp210 and for the nucleoporins. Thus the validity of the post-embedding quantitative approach was strengthened by these additional labeling experiments.

According to Akey and Radermacher (1993) the central channel of the NPC is occupied by the 'transporter' reported to have a double-barrel shape with a minimal radius of 16 nm at its center and a maximal radius of 21 nm at the cytoplasmic and nuclear faces. The large majority of antigenic nucleoporin sites found by us map to that region. Considering the fact that our specimens were chemically fixed and embedded prior to sectioning and labeling it appears improbable that the nuclear basket of the NPC might have collapsed during the preparative procedures to form the transporter, as suggested by Panté and Aebi (1994a,b). Also, the nucleoporin epitopes found by us in the NPC are very probably not constituted by 'vaults' because these RNPs do not contain nucleoporins (Kedersha and Rome, 1986). Thus, our observations may be taken as a support of the view that the transporter is a genuine and permanent component of the NPC.

Akey and Radermacher (1993) furthermore reported that the transporter contains a channel of approximately 4.5 nm radius. The limited resolution of our mapping technique precluded a discrimination of sub-structures. The only detail to be recognized (Fig. 7a) is that the density of nucleoporin epitopes appears to be somewhat larger towards the cytoplasmic face of the NPC. However, if the center of the NPC contains an abundance of highly glycosylated nucleoporins, as suggested by our observations, it cannot possibly have a completely solid and compact structure. Nucleoporins have been classified (Panté and Aebi, 1994) as peripheral membrane proteins and it appears impossible, in fact, to accommodate the large number of polar GlcNac residues of nucleoporins inside a compact protein complex. Thus, the NPC core is likely to have either a loosely woven texture or to be traversed by one or several GlcNac-lined and water-filled channel(s). On a qualitative level the latter is compatible with a large channel traversing the transporter (Akey and Radermacher, 1993).

Although the large majority of nucleoporin epitopes mapped to the NPC core, a few external epitopes were also observed (Figs 2,4). These extended some 30-40 nm into both the cytoplasmic and nuclear space and thus might be the equivalents of the nucleoporin epitopes found by the pre-embedding approach (Davis and Blobel, 1986, Akey and Goldfarb, 1989, Cordes et al., 1991, Panté and Aebi, 1993).

The authors acknowledge the excellent technical assistance of Mrs U. Malkus and the expert photographic work of Mrs G. Kiefermann and Mrs C. Jürgens. The polyclonal anti-p62 antibody was kindly donated by Prof. Dr Georg Krohne, Biozentrum der Universität, Würzburg, Germany. RL20 anti-gp210 monoclonal antibody was a generous gift from Dr Larry Gerace, The Scripps Research Institute, La Jolla, California, USA. Support by the Deutsche Forschungsgemeinschaft (grant Pe 138/11-2) is gratefully acknowledged.

REFERENCES

Adam, S. A., Sterne-Marr, R. and Gerace, L. (1990). Nuclear protein import in permeabilized mammalian cells requires soluble cytoplasmic factors. *J. Cell Biol.* **111**, 807-816.

Akey, C. W. and Goldfarb, D. S. (1989). Protein import through the nuclear pore is a multistep process. *J. Cell Biol.* **109**, 971-982.

Akey, C. W. (1990). Visualization of transport-related configurations of the nuclear pore transporter. *Biophys. J.* **58**, 341-355.

Akey, C. W. M. and Radermacher, M. (1993). Architecture of the Xenopus nuclear complex revealed by three-dimensional cryo-electron microscopy. *J. Cell Biol.* **122**, 1-19.

Aris, J. P. and Blobel, G. (1989). Yeast nuclear envelope proteins cross react with an antibody against mammalian pore complex proteins. *J Cell Biol.* **108**, 2059-2067.

Berrios, M., Fisher, P. A. and Matz, E. C. (1991). Localization of a myosin heavy chain-like polypeptide to *Drosophila* nuclear pore complexes. *Proc. Nat. Acad. Sci. USA* **88**, 219-223.

Carlemalm, E., Garavito, R. M. and Villiger, W. (1982). Resin development for electron microscopy and an analysis of embedding at low temperature. *J. Microsc.* **126**, 123-143.

Carmo-Fonseca, M., Kern, H. and Hurt, E. C. (1991). Human nucleoporin p62 and the essential yeast nuclear pore protein NSP1 show sequence homology and a similar domain organization. *Eur. J. Cell Biol.* **55**, 17-30.

Cordes, V., Waizenegger, I. and Krohne, G. (1991). Nuclear pore complex glycoprotein p62 of Xenopus laevis and mouse: cDNA cloning and identification of its glycosylated region. *Eur. J. Cell Biol.* **55**, 31-47.

Davis, L. I. and Blobel, G. (1986). Identification and characterization of a nuclear pore complex glycoprotein. *Cell* **45**, 699-709.

Davis, L. I. and Blobel, G. (1987). Nuclear pore complex contains a family of glycoproteins that includes p62: Glycosylation through a previously unidentified cellular pathway. *Proc. Nat. Acad. Sci. USA* **84**, 7552-7556.

Greber, U. F., Senior, A. and Gerace. L. (1990). A major glycoprotein of the nuclear pore complex is a membrane-spanning polypeptide with a large lumenal domain and a small cytoplasmic tail. *EMBO J.* **9**. 1495-1502.

Hinshaw, J. E., Carragher, B. O. and Milligan, R. A. (1992). Architecture and design of the nuclear pore complex. *Cell* **69**, 1133-1141.

Hinshaw, J. E. (1994). Architecture of the nuclear pore complex and its involvement in nucleocytoplasmic transport. *Biochem. Pharmacol.* **47**, 15-20.

Jarnik, M. and Aebi, U. (1991). Towards a more complete 3-D structure of the nuclear pore complex. *J. Struct. Biol.* **107**, 291-308.

Kedersha, N. L. and Rome, L. H. (1986). Isolation and characterization of a novel ribonucleoprotein particle: large particles contain a single species of small RNA. *J. Cell Biol.* **103**, 699-709.

Kedersha, N. L., Heuser, J. E., Chugani, D. C. and Rome, L. H. (1991): Vaults. III. Vault ribonuclein particles open into flower-like structures with octagonal symmetry. *J. Cell Biol.* **112**, 225-235.

Kellenberger, E. and Hayat, M. A. (1991). Some basic concepts for the choice

of method. In *Colloidal Gold. Principles, Methods, and Applications*, vol. 3 (ed. M. A. Hayat), pp. 1-31. Academic Press, New York.

Maul, G. G. (1977). The nuclear and the cytoplasmic pore complex: Structure, dynamics, distribution, and evolution. In *Int. Rev. Cytol.* suppl. 6 (ed. G. H. Bourne, J. F. Danielli and K. W. Jeon), pp. 75-186. Academic Press, New York, San Francisco, London.

Panté, N. and Aebi, U. (1993). The nuclear pore complex. *J. Cell Biol.* **122**, 977-984.

Panté, N. and Aebi, U. (1994a). Towards understanding the three-dimensional structure of the nuclear pore complex at the molecular level. *Curr. Opin. Struct. Biol.* **4**, 187-196.

Panté, N. and Aebi, U. (1994b) Toward the molecular details of the nuclear pore complex. *J. Struct. Biol.* **113**, 179-189.

Reichelt, R., Holzenburg, A., Buhle, E. L., Jarnik, M., Engel, A. and Aebi, U. (1990). Correlation between structure and mass distribution of the nuclear pore complex and of distinct pore complex components. *J. Cell Biol.* **110**, 883-894.

Ris, H. (1991). The 3-D structure of the nuclear pore complex as seen by high voltage electron microscopy and high resolution low voltage scanning electron microscopy. *EMSA Bull.* **21**, 54-56.

Ris, H. and Malecki, M. (1993). High resolution field emission scanning electron microscope imaging of internal cell structures after Epon extraction from sections: a new approach to correlative ultrastructural and immunocytochemical studies. *J. Struct. Biol.* **111**, 148-157.

Robards, A. W. and Wilson, A. J. (1993). Immunocytochemical techniques for TEM and SEM. In *Procedures in Electron Microscopy*. Wiley & Sons, Chichester, New York, Toronto.

Scheer, U., Dabauvalle, M.-C., Merkert, H. and Benevente, R. (1988). The nuclear envelope and the organization of the pore complex. In *Nucleocytoplasmic Transports* (ed. R. Peters), pp. 6-25. Academic Press, London.

Starr, C. M., D'Onofrio, M., Park, M. K. and Hanover, J. A. (1990). Primary sequence and heterologous expression of nuclear pore glycoprotein p62. *J. Cell Biol.* **110**, 1861-1871.

Unwin, P. N. T and Milligan, R. A. (1982). A large particle associated with the perimeter of the nuclear pore complex. *J. Cell Biol.* **93**, 63-75.

(Received 9 December 1994 - Accepted 23 June 1995)